

Combining multiple signals of an electromagnetic induction sensor to prospect land for metal objects

T. Saey^{1*}, M. Van Meirvenne¹, M. Dewilde², F. Wyffels², P. De Smedt¹,
E. Meerschman¹, M. M. Islam¹, F. Meeuws¹ and L. Cockx¹

¹ Research Group Soil Spatial Inventory Techniques, Faculty of Bioscience Engineering, Ghent University, Coupure 653, 9000 Gent, Belgium

² Vlaams Instituut voor het Onroerend Erfgoed – Dienst West-Vlaanderen, Iepersesteenweg 56, 8600 Diksmuide, Belgium

Received April 2010, revision accepted December 2010

ABSTRACT

Buried unexploded ammunition is a major problem on arable land in former battle areas. Many battlefields of the First World War (WWI) still contain a lot of unexploded shells just below the plough layer, posing serious threats to soil editors and trenchers. Electromagnetic induction (EMI) sensors have been used for a variety of agricultural and archaeological purposes to map the natural soil variability and to locate buried archaeological remains. Besides its sensitivity to variations in soil texture and anthropogenic disturbances, EMI proves to respond strongly to metal objects in the soil. Most EMI sensors rely on a single signal, with magnitude and sign of the metal anomalies differing according to the instruments coil distance and separation. The multi-coil EMI sensor, the DUALEM-21S, provides four simultaneous apparent electrical conductivity (*ECa*) signals enhancing significantly the possibilities for signal processing. To calibrate our instrument, we buried different masses of metal at different depths. The four *ECa* measurements showed a response to the metal objects down to 1.2 m. The measurements were subtracted by their gradual trend to obtain the local anomalies (ΔECa). A combination of these four ΔECa 's was used to amplify the signal response to metal, influenced by both depth and mass of the buried objects. At an intensively shelled former WWI battle field near Ypres (Belgium), a detailed prospection was conducted with the DUALEM-21S. Based on our multi-signal procedure, we located 40 positions, 20 where we predicted buried metal and 20 where we expected that no metal was present within 1.2 m depth. There were no false negative predictions and at the 20 locations where we expected metal, shells up to 90 kg were excavated. As a final outcome we produced a map with predictions of the mass of metal objects in the soil assuming a fixed depth and alternatively a map with predictions of the depth of metal objects assuming a given mass.

Apart from their potential for agricultural and archaeological investigations, multi-*ECa* signals were shown to be useful for locating metal objects, like unexploded WWI shells, in the top 1.2 m of soil.

INTRODUCTION

Electromagnetic (EMI) methods for near-surface investigations have undergone rapid improvements over the past years. A number of new applications have appeared in precision agriculture and archaeological prospection. In precision agriculture, the measurement of apparent soil electrical conductivity (*ECa*) with EMI is a technology that has become an invaluable tool for identifying the soil physico-chemical properties influencing crop yield patterns and for establishing the spatial variation of these soil properties (Corwin and Lesch 2005). In archaeology, geophysical prospecting appears as a means to obtain a broader

description of the archaeological landscape. Indeed, all the buried structures that are potentially detectable will be detected, whatever their nature and age (Bossuet *et al.* 2001). Despite the fact that EMI is less frequently used in archaeology, measurements of the apparent magnetic susceptibility (*MSa*) with EMI exhibit similar anomalies due to magnetic susceptible materials such as gradiometers (Simpson *et al.* 2009). The great advantage of using EMI is the low cost of sampling data at sufficient intensities to provide accurate mapped information. It is a rapid, non-invasive method for collecting soil *ECa* and *MSa* information (Saey *et al.* 2009b). Moreover, EMI proves useful for the detection and location of buried metal objects (Casey and Baertlein 1999).

* timothy.saey@ugent.be

During the First World War (WWI), fought between August 1914 and November 1918, an estimated 1.45 billion shells were fired by the combined German, French and British armies on all fronts (Prentiss 1937). In the war zone around Ypres, the exact number of shells fired during WWI remains unrecorded but it must have been several tens of millions (Van Meirvenne *et al.* 2008). Karg (2005) estimated that about 10–15 % of them remain unexploded. Although this former front zone has continuously been cleaned-up since 1919, unexploded WWI ammunition is still found frequently during soil tillage and archaeological excavations because deeper objects move to the surface or because farmers plough deeper (Masters and Stichelbaut 2009). Consequently, it is important to detect metal below the plough layer. The Belgian army maintains a permanent unit available to collect and dismantle former WWI shells. About 250 tons of such material is being processed annually.

Although the use of magnetometry permits detection of ferrous metallic objects at the greatest depths, the real problem is generally not the detection at great depths but the identification of the target itself. Generally, the number of unexploded targets can be extremely small compared to the total number of retained targets with magnetometry. Electromagnetic induction surveys have been successful in detecting subsurface ferrous and non-ferrous metallic objects and these surveys are a mainstay amongst technologies currently utilized in unexploded ordnance (UXO) clearance projects. Mostly, time-domain electromagnetic instruments are used for UXO detection. They are able to measure at different times, thereby characterizing the metallic object (Pasion 1999). Recently, multi-array frequency-domain EMI systems have been applied for detecting unexploded shells. Huang *et al.* (2007) described a new broadband EMI array system with a single transmitter and seven pairs of receivers to delineate unexploded ordnance. Less research has been done to exploit the possibilities of the DUALEM EMI soil sensors (DUALEM Inc., Milton, Ontario, Canada) for metal detection

and characterization. Generally, these sensors were used for the time-effective prospection of large areas for agricultural (Abdu *et al.* 2008), geomorphological (Saey *et al.* 2009a) and archaeological (Simpson *et al.* 2009) purposes. On arable fields situated in historical battlefields, these EMI sensors could indicate the presence of buried shells supplementary to their agricultural and archaeological value.

The main objective of this study was to investigate the ability of a multi-array electromagnetic induction sensor in detecting metal objects below the plough layer. Therefore, a procedure was developed: 1) to search a combination of the multiple signals that yields a unique response of the metal objects, 2) to relate the combined signals to the depth and mass of the objects and 3) to evaluate the applicability of this procedure at a former WWI battle field.

MATERIALS AND METHODS

Metal detecting

Most modern metal detectors are based on the principle of electromagnetic induction. Generally, they use separate transmit/receive circuits and operate in a very low frequency-region, typically between a few kHz and a few tens of kHz (say 1–50 kHz). An alternating current passing through the transmitter coil generates a time-varying magnetic field, the primary field. This primary field induces surface currents on the target and eddy currents in the soil, which in turn generate a secondary magnetic field. Both the primary and the secondary field create currents through the receiver coil, from which the voltage is measured. For time-domain transmission, as time elapses, the surface currents diffuse inwards the object and the observed secondary field consequently decays. The rate of decay is determined by the target's conductivity, magnetic permeability, shape and size. Therefore, information on the target's nature can be gathered by analysing the decay by measuring the secondary field at different times, done with time-domain EMI instruments.

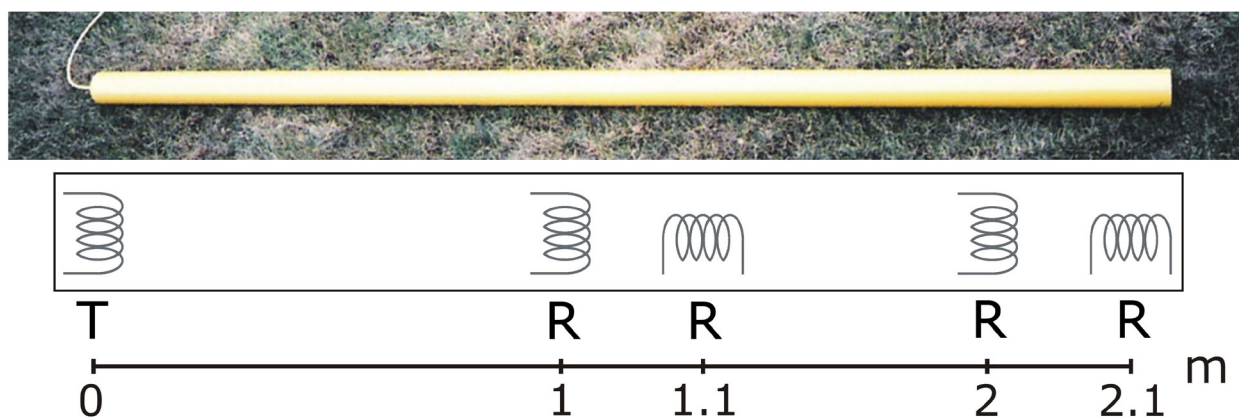


FIGURE 1
Transmitter (T) and receiver (R) orientations and coil spacings of the DUALEM-21S instrument.

TABLE 1

Technical specifications of the DUALEM-21S instrument (Dualem Inc. 2006)

EMI systems	vertical transmitter and receiver, perpendicular transmitter and receiver;
System configuration	1 m vertical / 1.1 m perpendicular and 2 m vertical / 2.1 m perpendicular (DUALEM-21S) transmitter-receiver separation, operating at 9 kHz;
Measured quantities	Vertical and perpendicular conductivity (ECa) in $mS\ m^{-1}$, vertical and perpendicular in-phase (MSa) in ppt
Measurement ranges	ECa : $\pm 3000\ mS\ m^{-1}$, MSa : $\pm 300\ ppt$;
RMS noise levels at 1-Hz data rate	ECa : $\pm 0.25\ mS\ m^{-1}$, MSa : $\pm 0.005\ ppt$ for 1 m coil configurations ECa : $\pm 0.1\ mS\ m^{-1}$, MSa : $\pm 0.02\ ppt$ for 2 m coil configurations;
Data rates	Manual, or continuous at rates between 0.1–8 Hz;
Digital signal processor	Custom built, with digital clock, thermometer, pitch sensor, roll sensor, RS-232 port and receive/transmit LEDs;
Data capacity	65 000 records of time, survey documentation and measured quantities;
Output format	Proprietary or NMEA-compatible, using ASCII characters through RS-232 port;

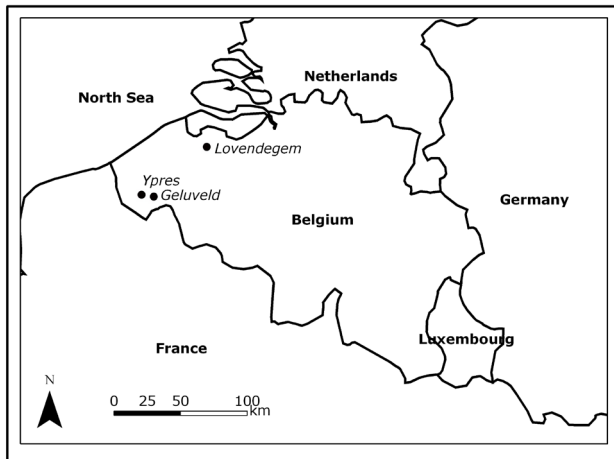


FIGURE 2
Localization of the Lovendegem and Geluvelde study sites in Belgium.

Frequency-domain EMI sensors measure the secondary field at one time, frequently with various receiver coils at different distances from the transmitter coil. The DUALEM-21S sensor consists of a 2.41 m long tube with one transmitter coil and four receiver coils (Saey *et al.* 2009a). In the quadrature-phase response, the ratio of the secondary over the primary field is proportional to the apparent electrical conductivity (ECa) of the soil (McNeill 1980); in the in-phase response, this ratio is proportional to the apparent magnetic susceptibility (MSa) (McNeill 1980). The transmitter coil is located at one end, the receiver coils are at 1 m, 1.1 m, 2 m and 2.1 m spaced from the transmitter coil (Fig. 1). The 1 m and 2 m transmitter-receiver pairs form a vertical

dipole mode (1V and 2V) (normally called HCP), while the 1.1 m and 2.1 m pairs form a perpendicular dipole mode (1.1P and 2.1P). The quadrature-phase magnetic field is simultaneously measured in these four coil configurations. The DUALEM-21S simultaneously measures the ECa in the vertical dipole mode with coil spacings of 1 m ($ECa_{v,1}$) and 2 m ($ECa_{v,2}$), in the perpendicular dipole mode with coil spacings of 1.1 m ($ECa_{p,1.1}$) and 2.1 m ($ECa_{p,2.1}$) and the apparent magnetic susceptibility (MSa) in the same four coil orientations (Table 1). The combination of the four simultaneous ECa measurements shows large potential for the identification and characterization of underground features (Saey *et al.* 2009a). The noise level of the DUALEM-21S $MSa_{p,1.1}$ and $MSa_{p,2.1}$ measurements is very high, diminishing the possibilities for combining the four simultaneous magnetic susceptibility measurements.

The DUALEM-21S was mounted on a sled pulled by an all terrain vehicle (ATV), which drove with a speed of 3–5 $km\ h^{-1}$. Every 8th fraction of a second, the four ECa and MSa measurements were recorded by a field computer. A Trimble AgGPS332, with Omnistar correction, was used to georeference the measurements with a pass-to-pass accuracy of $\pm 0.10\ m$. Measurements on the calibration and validation site were taken along parallel lines with an in-between distance of respectively 0.30 m and 0.85 m. Driving was supported by a Trimble Lightbar Guidance System. The large number of measurements, collected in a relatively short time (19 April 2008), provides a comprehensive coverage of the sites.

Calibration site

Our 0.1 ha calibration site was located in Lovendegem (with central coordinates: 51°07'19"N, 3°37'05"E), in the province of

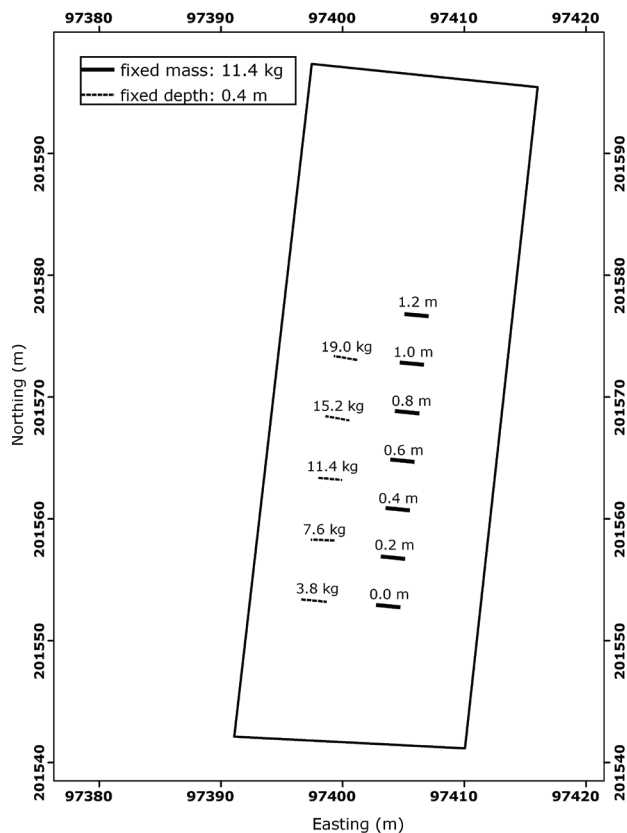


FIGURE 3
Situation of the metal bars with different m buried at different z in the soil.

East-Flanders, Belgium (Fig. 2). At this site, topsoil texture is loamy sand. Groups of three metal bars (chrome metal bars with length 2m and diameter 12 mm) with a total fixed mass (m) of 11.4 kg were put in the soil at depths (z) of 0.0 m, 0.2 m, 0.4 m, 0.6 m, 0.8 m, 1.0 m and 1.2 m below surface. Additionally, metal bars were buried at a fixed z of 0.4 m but with an increasing m of 3.8 kg, 7.6 kg, 11.4 kg, 15.2 kg and 19.0 kg (Fig. 3). East of these two transects with differing depth and mass, other metal objects were buried in the soil. These were irrelevant for this research. This design was created to quantify the effect of m and z on the measurements with the multi-signal EMI sensor. We did not consider the effect of the targets shape and conductivity on the EMI measurements. At this site, DUALEM-21S measurements were performed with the instrument orientated perpendicular to the metal bars. The distance in-between the tracks or middle of the instrument was 0.3 m.

Validation site

The 2.6 ha validation site was a former WWI battle field, located in Geluvelde (with central coordinates: 50°50'23"N, 2°59'23"E), in the south-west of the province of West-Flanders, Belgium (Fig. 2). At our site, the topsoil texture consists of sandy/silty Pleistocene wind-blown sediments. The substrate directly located below the sandy loam is composed of a range of marine sandy

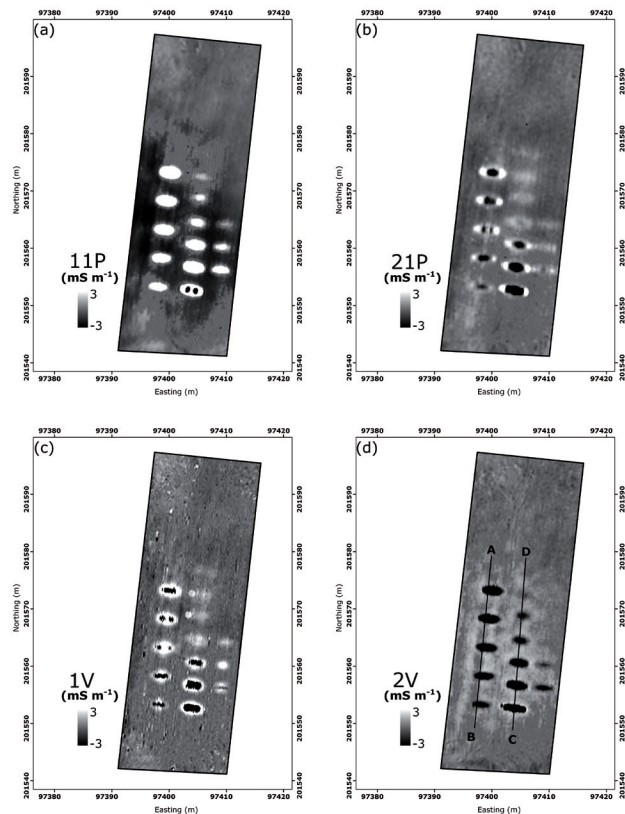


FIGURE 4
 $\Delta ECa_{p,1.1}$ with indication of m and z of the metal bars in the soil (a), $\Delta ECa_{p,2.1}$ (b), $\Delta ECa_{v,1}$ (c) and $\Delta ECa_{v,2}$ with delineation of transects AB and DC (d) at the Lovendegem calibration site.

depositions dating from the Early Eocene, with embedded clay patches. This site was bombed intensively during WWI. It was situated on the 'Geluvelde plateau', south-east of Ypres. Due to the intense bombardments during WWI, a large amount of shell fragments and unexploded ammunition was expected in the subsoil of this arable field. The farmer frequently surfaces unexploded shells during tillage, confirming this hypothesis. At this site, the measurements were performed with the instrument parallel to the measurement direction. The distance in-between the tracks was 0.85 m.

Interpolation and filtering

To estimate the ECa at unsampled locations, ordinary point kriging (OK) was used as an interpolation method. OK provides estimates of a variable at any unsampled location using a linear combination of observations within a predefined neighbourhood around this location (Goovaerts 1997). At our calibration site, a minimum of four neighbours were used within a circular search area with a radius of 1 m around the location being interpolated. The data points were interpolated to a grid of 0.1 m \times 0.1 m. At our validation site, a minimum of 4 neighbours were used within a circular search area with a radius of 4 m; interpolation was done on a 0.2 m \times 0.2 m grid.

The spatial structure of the variables is represented by variogram models, which were used to assign weights to the neighbouring measurement points. With the ‘Variogram Estimation and Spatial Prediction with Error’ (VESPER) program, theoretical variogram models were fit to the experimental global variograms (Minasny *et al.* 2005).

To remove the influence of the natural soil variability on the measurements and focus on the local anomalies in the data, a filtering procedure was followed. The extreme values were converted to the mean value of the neighbouring measurement points within a circular search area with a radius of 10 m (ECa_{filtered}). Afterwards, this gradual trend was subtracted from the original ECa measurements to highlight the local anomalies (ΔECa):

$$\Delta ECa = (ECa - ECa_{\text{filtered}}). \quad (1)$$

Validation observations

At the Geluvelde study site, metal objects were dug out in layers of 0.2 m in an area of 0.8 m by 0.8 m at 40 selected locations. For each successive layer, the encountered metal pieces were collected and weighted. This provided an assessment of the z and m of the metal objects at the visited locations.

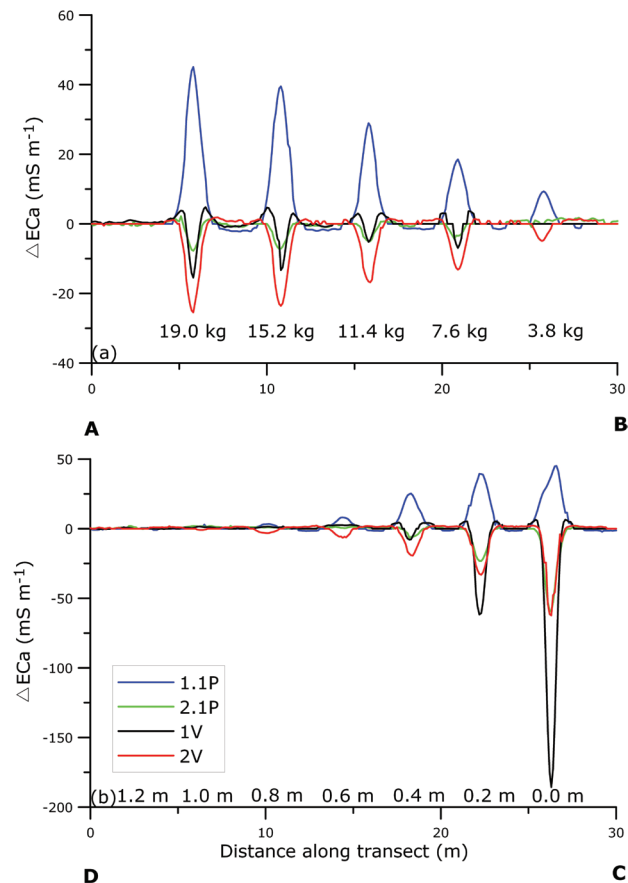


FIGURE 5 ΔECa values along transect AB (a) and along transect DC (b).

RESULTS AND DISCUSSION

ECa survey

At the calibration site, homogeneous ECa of 10 mS m^{-1} was subtracted from the measurements to obtain the ΔECa . The four ΔECa maps of the calibration site are shown in Fig. 4. Each signal responded in a different way to the buried metal bars, at different z and with different m . The variation in magnitude of the response can be attributed to the z and m of the buried metal; the differences in sign of the anomalies can be assigned to the specific coil configurations.

Transects

To quantify the influence of the metal bars on the measurements, we focused on the ΔECa values along two transects AB and DC (Fig. 4d). On transect AB, the amount of metal bars or m at a fixed z of 0.4 m varied, while along transect DC, z of a metal mass of 11.4 kg varied. Figure 5 shows the ΔECa transects AB and DC, with varying m and z across the two transects. All ΔECa 's were sensitive to differences in m (transect AB) and z (transect DC) of the metal bars in the soil. $\Delta ECa_{v,1}$ was most affected by shallow objects, while $\Delta ECa_{p,1,1}$ and $\Delta ECa_{v,2}$ experienced influences up to $z = 1.0 \text{ m}$. Besides, metal objects in the subsoil result in positive $\Delta ECa_{p,1,1}$ peaks and negative $\Delta ECa_{p,2,1}$, $\Delta ECa_{v,1}$ and $\Delta ECa_{v,2}$ peaks. To improve the contrast between the metal objects and the non-metallic background, the four ΔECa 's were optimally combined to ‘fused electromagnetic metal prediction (FEMP)’:

$$\text{FEMP} = a \cdot \Delta ECa_{p,1,1} - b \cdot \Delta ECa_{p,2,1} - c \cdot \Delta ECa_{v,1} - d \cdot \Delta ECa_{v,2}. \quad (2)$$

with a , b , c and d the weighting coefficients.

The sign of the weighing coefficients can be justified by the positive $\Delta ECa_{p,1,1}$ and negative $\Delta ECa_{p,2,1}$, $\Delta ECa_{v,1}$ and $\Delta ECa_{v,2}$ peaks above the metal bars. The weighting coefficients a , b , c and d were solved by equating the fused FEMP for the 11.4 kg peak at transect AB ($z = 0.4 \text{ m}$) to the 0.4 m peak at transect DC ($m = 11.4 \text{ kg}$) besides fixing them to a value of 100 mS m^{-1} ; by equating FEMP to 0 mS m^{-1} for metal at 1.2 m depth because the metal anomalies are 0 at this depth; and by fixing coefficient b to 1 as a starting condition. Finally, the following combination was found:

$$\text{FEMP} = 2.05 \cdot \Delta ECa_{p,1,1} - 1 \cdot \Delta ECa_{p,2,1} - 0.82 \cdot \Delta ECa_{v,1} - 1.89 \cdot \Delta ECa_{v,2}. \quad (3)$$

Both $\Delta ECa_{p,1,1}$ and $\Delta ECa_{v,2}$ receive the greatest weight in the FEMP while $\Delta ECa_{v,1}$ receives the smallest weight. As such, the values of the solved weighting coefficients correspond well to the peaks in the ΔECa (Fig. 5). The higher the m of the objects on transect AB, the higher the FEMP. The closer the objects are to the surface on transect CD, the higher the FEMP. Finally, the combination gives positive unique anomalies for metal objects down to 1.0 m (Fig. 6). Metal is expected to be present at positive FEMP peaks. Negative FEMP values predict the absence of metal objects in the soil profile.

The value of the FEMP at the centre of each group of metal bars was related to m and z of the metal bars. A linear relationship was found between the FEMP peak values and m (Fig. 7a):

$$m = 0.108 \cdot \text{FEMP} + 0.651, \tag{4}$$

with an R^2 of 0.98 ($n = 5$).

A log-linear relationship was found between the FEMP peak values and z (Fig. 7b):

$$z = -0.213 \cdot \ln(\text{FEMP}) + 1.324, \tag{5}$$

with an R^2 of 0.99 ($n = 5$).

Validation

The developed methodology was applied at the Geluvelde study site. Figure 8 gives the ECa measurements with the DUALEM-21S at the Geluvelde study site, ranging between 10–40 mS m^{-1} . The ECa values increase with increasing DOE (depth of exploration or the depth at 70% cumulative response (Saey *et al.* 2009a)) for the specific coil configurations (from Fig. 8a–d), so the

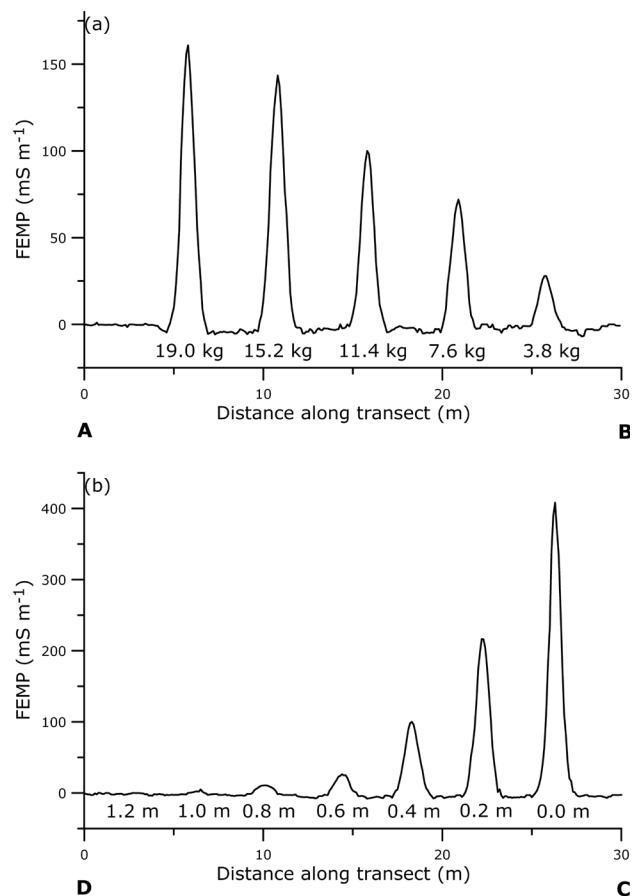


FIGURE 6 FEMP $\text{FEMP} = 2.05 \cdot \Delta ECa_{p,1.1} - 1 \cdot \Delta ECa_{p,2.1} - 0.82 \cdot \Delta ECa_{v,1} - 1.89 \cdot ECa_{v,2}$ values along transect AB (a) and along transect DC (b).

larger the measured soil volume, the higher the conductivity, indicating a high conductive layer to be present in the deeper soil. The speckles on the measurements are probably all due to bomb wefts with remaining shrapnel and unexploded ammunition. To obtain unique values of the metal anomalies, the four ΔECa maps were combined to the FEMP, shown in Fig. 9. Many speckles of high FEMP were observed at the site. So a lot of buried metal objects can be expected.

To validate equations (4) and (5) established at the Lovendegem study site, 40 locations were designated based on the FEMP map. From these 40 locations, 20 were predicted to be ‘magnetic metal-empty’ ($\text{FEMP} < 0$) and 20 were modelled to contain

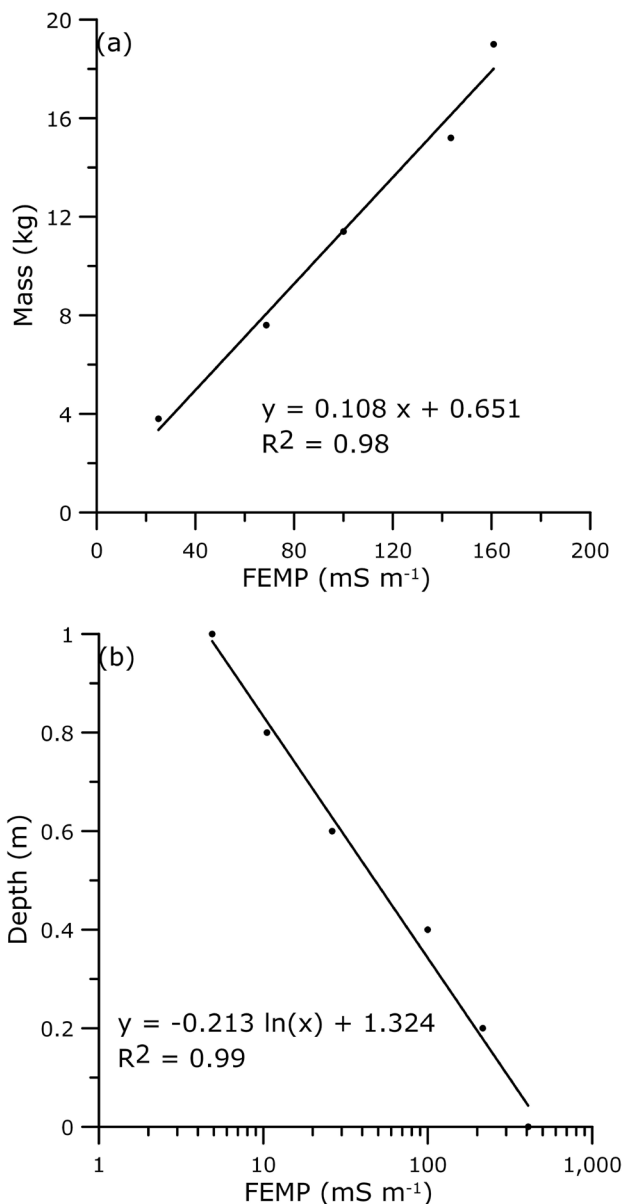


FIGURE 7 m as a function of the FEMP of the metal bars along transect AB (a) and z as a function of FEMP along transect DC (b)

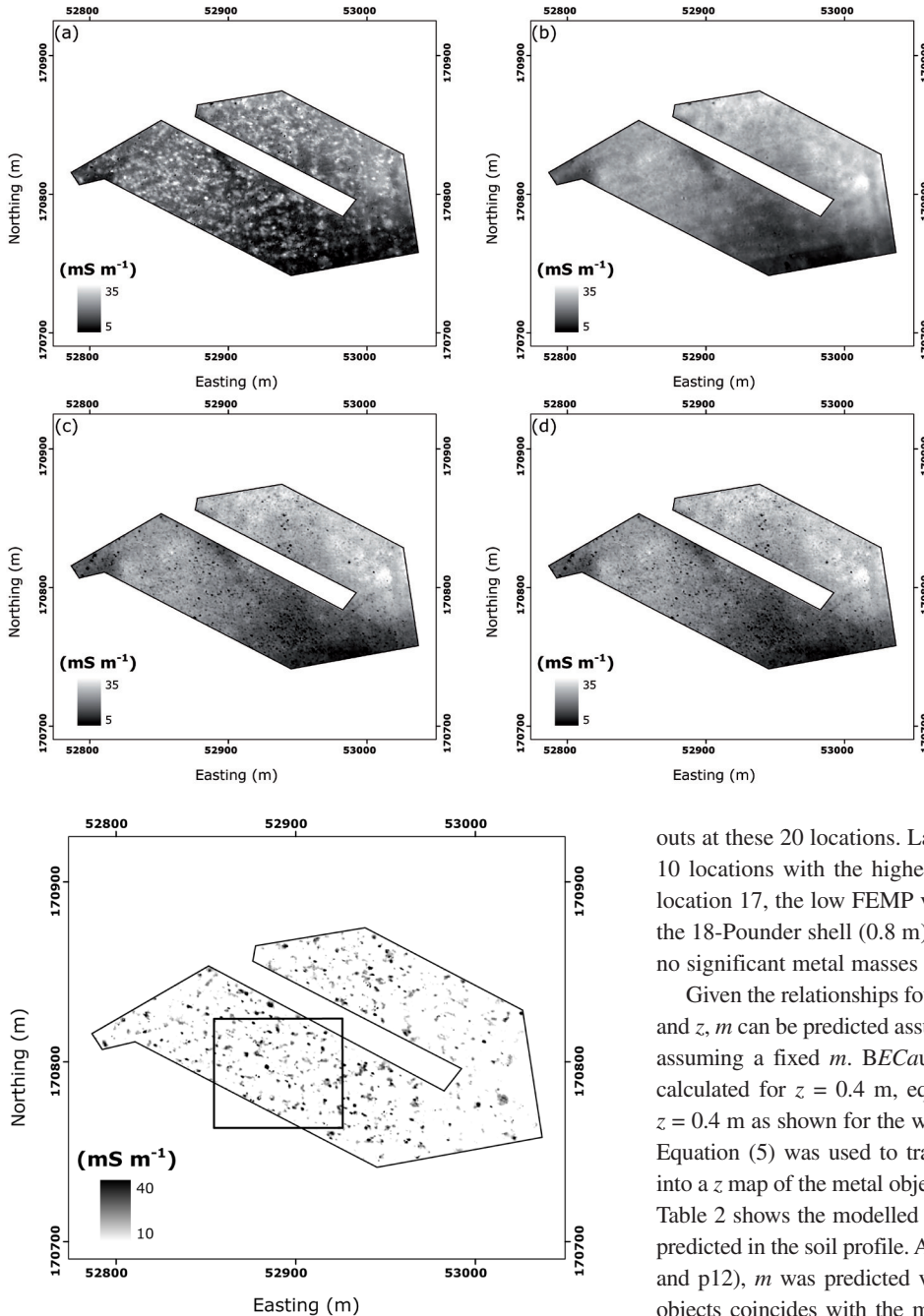


FIGURE 8
 $ECa_{p,1,1}$ (a), $ECa_{p,2,1}$ (b), $ECa_{v,1}$ (c)
 and $ECa_{v,2}$ (d) measurements with the
 DUALEM-21S instrument at the
 Geluveld study site.

FIGURE 9
 FEMP map at the Geluveld study site with indication of a detail window.

buried metal. The latter 20 locations were spread out over the range of FEMP values, from 6–197 $mS\ m^{-1}$.

According to the excavations, the 20 locations where no metal was predicted in the subsoil proved ‘magnetic metal-empty’. The 20 spots with predicted metal contained pieces of varying mass at different depths in their profile. The metal pieces were weighed and their z was recorded. Table 2 gives the inventory of dug-

outs at these 20 locations. Large shell remains were found at the 10 locations with the highest FEMP values ($> 47\ mS\ m^{-1}$). At location 17, the low FEMP value was attributed to the large z of the 18-Pounder shell (0.8 m). Below a FEMP value of 6 $mS\ m^{-1}$, no significant metal masses were found.

Given the relationships found between the FEMP values and m and z , m can be predicted assuming a fixed z , or z can be modelled assuming a fixed m . Because the relationship m - FEMP was calculated for $z = 0.4\ m$, equation (4) was used to model m at $z = 0.4\ m$ as shown for the window indicated in Fig. 9 (Fig. 10a). Equation (5) was used to transform the logarithmic FEMP map into a z map of the metal objects assuming $m = 11.4\ kg$ (Fig. 10b). Table 2 shows the modelled z and m for the locations with metal predicted in the soil profile. At some locations (for example p3, p4 and p12), m was predicted very well, because the depth of the objects coincides with the modelling depth. At most other locations, z was less accurate, either because the depth of the objects differed from the 0.4 m, or because metal was spread at multiple depth intervals. The greater part of the metal objects, assuming $m = 11.4\ kg$, was predicted to be located between 0.4–0.8 m depth. However, the greater part of the objects was situated in-between the soil surface and 0.6 m depth. Therefore, the z predictions proved to be less acceptable than the m modellings.

CONCLUSIONS

We concluded that the following procedure proved successful for delineating and characterizing metal objects in the subsoil:

TABLE 2

Inventory of the metal objects in the subsoil at the 20 locations with metal predicted in the subsoil (p1–p20) with their accompanied FEMP value (in bold: shell remains) (m : mass and z : depth)

Location	m (kg)	m (kg)	m (kg)	m (kg)	FEMP (mS m^{-1}) Value	z^* (m)	m^* (kg)	Identification
	0-0.4 m	0.4-0.6 m	0.6-0.8 m	> 0.8 m		$m = 11.4$ kg	$z = 0.4$ m	
p1	90.4	1.7	–	–	197	0.20	21.9	8-inch Howitzer
p2	3.9	–	–	–	155	0.25	17.4	18-Pounder
p3	16.3	–	–	–	120	0.30	13.6	4.5-inch Howitzer
p4	15.8	–	–	–	111	0.32	12.6	4.5-inch Howitzer
p5	3.7	2.5	–	–	94	0.36	10.8	18-Pounder
p6	–	0.8	30.9	–	65	0.43	7.7	60-Pounder
p7	4.6	5.8	1.5	10.8	57	0.46	6.8	18-Pounders
p8	0.9	–	–	–	55	0.47	6.6	shrapnel
p9	4.8	0.5	2.9	–	47	0.50	5.7	18-Pounder
p10	0.4	2.0	3.4	1.5	47	0.50	5.7	shrapnel
p11	0.5	1.2	–	–	24	0.65	3.2	shrapnel
p12	–	2.5	–	–	24	0.65	3.2	shrapnel
p13	2.0	–	–	–	19	0.70	2.7	shrapnel
p14	1.8	0.4	–	–	16	0.73	2.4	shrapnel
p15	–	0.02	–	–	14	0.76	2.2	shrapnel
p16	–	1.4	–	–	14	0.76	2.2	shrapnel
p17	0.07	0.2	6.3	–	10	0.83	1.7	18-Pounder
p18	0.02	–	–	–	8	0.88	1.5	shrapnel
p19	0.08	0.2	–	–	7	0.91	1.4	shrapnel
p20	0.1	–	–	–	6	0.94	1.3	shrapnel

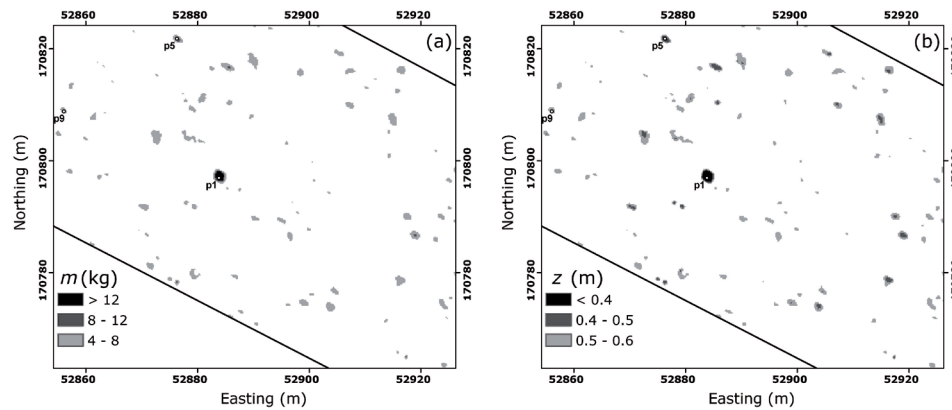


FIGURE 10

m of the metal objects at the detail window in Fig. 9 assuming $z = 0.4$ m (a) and z assuming $m = 11.4$ kg (b).

- 1 The four ECa measurements of the DUALEM-21S were subtracted by their filtered values and the resulting ΔECa maps were combined to the $FEMP = 2.05 \cdot \Delta ECa_{p,1,1} - 1 \cdot \Delta ECa_{p,2,1} - 0.82 \cdot \Delta ECa_{v,1} - 1.89 \cdot ECa_{v,2}$ to obtain a unique signal from buried metal objects with different m and z .
- 2 A clear relationship exists between the FEMP values and m and z .
- 3 At a WWI battlefield, large shell remains were encountered at locations with a FEMP value ongoing 47 mS m^{-1} . No metal could be found at locations with negative FEMP. Additionally,

z predictions were made assuming a fixed m of the metal bodies and m was predicted assuming a fixed z .

This study confirmed the benefit of the combination of our multi-signal DUALEM-21S measurements in delineating buried metal objects besides their potency for agricultural and archaeological purposes. Depth and mass predictions proved more difficult, although some rough estimation could be made.

ACKNOWLEDGEMENTS

This research was supported by the Fund for Scientific Research-Flanders (FWO-Vlaanderen). The authors thank Mr C. Decuyper

for granting access to his field and Mr H. Vermeersch, Mr D. Simpson and the collaborators of the Vlaams Instituut voor het Onroerend Erfgoed (VIOE) for their labour in the field.

REFERENCES

- Abdu H., Robinson D.A. and Jones S.B. 2007. Comparing bulk soil electrical conductivity determination using the DUALEM-1S and EM38-DD electromagnetic induction instruments. *Soil Science Society of America Journal* **71**, 189–196.
- Bossuet G., Camerlynck C., Brehonnet C. and Petit C. 2001. Magnetic prospecting of diachronic structures (antiquity to First World War) on the site of the sanctuary of Ribemont-sur-Ancre (Somme, France). *Archaeological Prospection* **8**, 67–77.
- Casey K.F. and Baertlein B.A. 1999. An overview of electromagnetic methods in subsurface detection. In: *Detection and Identification of Visually Obscured Objects* (ed. C.E. Baum), pp. 9–46. Taylor & Francis.
- Corwin D.L. and Lesch S.M. 2005. Apparent soil electrical conductivity measurements in agriculture. *Computers and Electronics in Agriculture* **46**, 11–43.
- Dualem Inc. 2006. *DUALEM-1S and DUALEM-2S user's manual*.
- Goovaerts P. 1997. *Geostatistics for Natural Resources Evaluation*. Oxford University Press.
- Huang H., San Filippo B., Oren A. and Won I.J. 2007. Coaxial coil towed EMI sensor array for UXO detection and characterization. *Journal of Applied Geophysics* **61**, 217–226.
- Karg F. 2005. Consideration of toxic metabolites from explosives & chemical warfare agents on polluted military and armament sites for health risk assessments. In: *Consoil 2005 Proceedings* (eds O. Uhlmann, G. Annokkée and F. Arendt), pp. 710–720. Forschungszentrum Karlsruhe.
- Masters P. and Stichelbaut B. 2009. From the air to beneath the soil – Revealing and mapping Great War trenches at Ploegsteert (Comines – Warneton), Belgium. *Archaeological Prospection* **16**, 279–285.
- McNeill J.D. 1980. *Electromagnetic terrain conductivity measurement at low induction numbers*. Technical Note TN-6, Geonics Ltd, Mississauga, Ontario, Canada.
- Minasny B., McBratney A.B. and Whelan B.M. 2005. *VESPER version 1.62*. Australian Centre for Precision Agriculture, McMillan Building A05, The University of Sydney, NSW 2006. (<http://www.usyd.edu.au/su/agric/acpa>).
- Pasion L.R. 1999. *Detecting unexploded ordnance with time domain electromagnetic induction*. Master thesis, The University of British Columbia.
- Prentiss A.M. 1937. *Chemicals in War: A Treatise on Chemical Warfare*. McGraw-Hill.
- Saey T., Simpson D., Vermeersch H., Cockx L. and Van Meirvenne M. 2009a. Comparing the EM38DD and DUALEM-21S Sensors for Depth-to-Clay Mapping. *Soil Science Society of America Journal* **73**, 7–12.
- Saey T., Van Meirvenne M., Vermeersch H., Ameloot N. and Cockx L. 2009b. A pedotransfer function to evaluate the soil profile textural heterogeneity using proximally sensed apparent electrical conductivity. *Geoderma* **150**, 389–395.
- Simpson D., Lehouck A., Verdonck L., Vermeersch H., Van Meirvenne M., Bourgeois J. *et al.* 2009. Comparison between electromagnetic induction and fluxgate gradiometer measurements on the buried remains of a 17th century castle. *Journal of Applied Geophysics* **68**, 294–300.
- Van Meirvenne M., Meklit T., Verstraete S., De Boever M. and Tack F. 2008. Could shelling in the First World War have increased copper concentrations in the soil around Ypres? *European Journal of Soil Science* **59**, 372–379.

NEAR SURFACE GEOPHYSICS:

Choosing the Right Magnetometer

Magnetic applications in near surface geophysics are broad: mineral exploration, archaeology, environmental & engineering, geological hazards, UXO detection. It is important to choose the right solution.

The Versatility of Overhauser

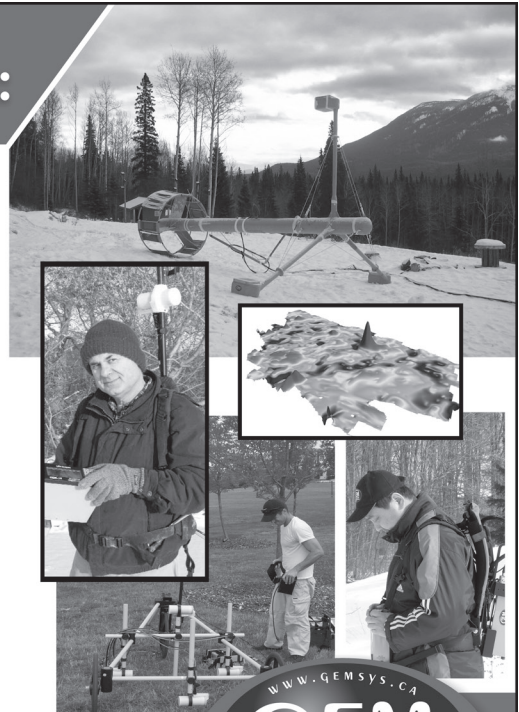
For general work and teaching the Overhauser instrument is ideal: low power consumption, 5 Hz sampling, no directional errors, optional sensitivity 0.015 nT @ 1 Hz. Overhauser is made for efficiency with its light weight, low power consumption, robust console and intelligent surveying options.

The Power of Potassium

For sensitive work and research the ultimate solution is the Potassium instrument. The K-Mag samples at a leading 20 Hz for acquisition of high resolution results, sensitivity 0.0007 nT/√Hz (70mm cell). It features minimal directional errors and high gradient tolerance for culturally "noisy" projects.

Find Your Solution

To work with diverse earth science challenges you can choose any of GEM's systems delivering clear benefits.

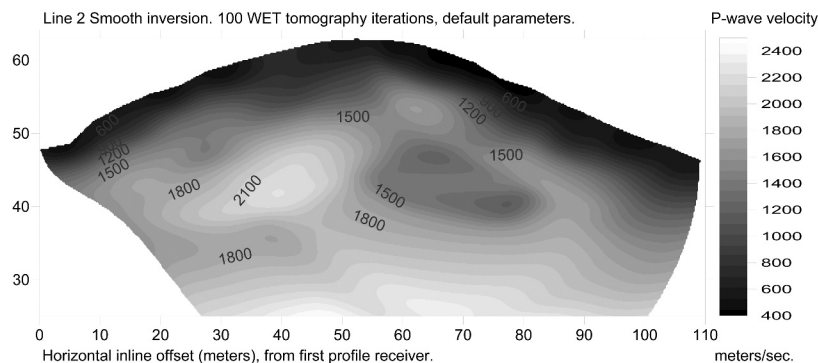


Web: www.gemsys.ca
Email: info@gemsys.ca
Phone: +1 905 752 2202

WWW.GEMSYS.CA
GEM
SYSTEMS
ADVANCED MAGNETOMETERS

Our World is Magnetic.

INTELLIGENT RESOURCES INC. offers RAYFRACT® Seismic Refraction & Borehole Tomography software : velocity structure imaging for engineering and exploration



Intelligent Resources Inc.
142-757 West Hastings Street
Vancouver B.C. V6C 1A1
Canada

Phone +1 604 782-9845
Fax +1 604 408-8678
Web <http://rayfract.com>
E-mail sales@rayfract.com

200 full licenses sold.

Our Rayfract® travelttime tomography software models refraction, transmission and diffraction of seismic waves. Just define 2D profile geometry, import or pick first breaks then obtain optimal interpretations automatically. Supports extreme topography and strong lateral velocity variation. Handles velocity inversions. Smooth inversion of downhole VSP and crosshole surveys, with constant-velocity initial model. Includes conventional Plus-Minus, Wavefront methods. Allows import of SEG-2, ABEM Terraloc Mark III, Bison 9000 Series binary trace data. Can read many third-party ASCII file formats with first breaks and recording geometry. The price of an end user license remains unchanged at US \$ 2,200.00 including one year of support. We offer a price reduction of 20% to academic and non-profit organizations. Send us a test profile for free interpretation. Visit our web site for latest release notes, manual, free trial, tutorials and benchmark comparisons. You may rent our software. Resellers are welcome.

Copyright © 1996-2010 Intelligent Resources Inc. RAYFRACT is a registered trademark of Intelligent Resources Inc. Canadian Business Number 86680 1236. British Columbia Incorporation Certificate No. 605136. Requires Golden Software's Surfer for plotting.